Calibration Setup for Ultralow-Current Transresistance Amplifiers

Calibration setup for ultralow-current transresistance amplifiers

Ilaria Finardi, and Luca Callegaro

Abstract

We describe a setup for the calibration of the transresistance gain of low-current amplifiers, based on the capacitance-charging method. The calibration can be performed in the current range of typical interest for electron counting experiments. The setup implementation is simple and rugged, and is suitable to be embedded in larger experiments where the amplifier is employed. The calibrated transresistance is traceable to the units of capacitance and time. Two different calibration modes were tested: with dc current (obtained using a custom-made piecewise-linear ramp generator) and with low-frequency sinewave current (using a commercial generator). The relative base accuracy of the implementation is in the 10^{-5} range.

Index Terms

Metrology, Current measurement, Amplifiers, Gain measurement, Calibration, Capacitance.

I. Introduction

The announced future revision of the International System of Units (SI) [1], [2], and the redefinition of the unit of electric current ampere in terms of the elementary charge, have raised the interest on dc current generation with electron-counting experiments. In these experiments the current magnitudes are typically below the nA, and have to be amplified by large factors.

Measurements of such low currents with ultimate accuracy were performed in the last twenty years with purpose-built cryogenic current comparators (CCC) having large turn ratios [3]–[5]. The Physikalisch-Technische Bundesanstalt (PTB), Germany, has developed a special current amplifier, the ULCA-1 [6], having a highly stable current gain [7], which can be calibrated with a CCC bridge [5]. These measurement setups achieve uncertainties at the 10^{-7} level but require non-commercial instrumentation, a cryogenic environment, and trained operators.

In the investigation of novel devices for electron-counting experiments, typical measurement setups involve commercial ultralow-current transresistance amplifiers [8]–[10], having typical transresistance gain R ranging from $\mathrm{G\Omega}$ to several $\mathrm{T\Omega}$.

In the following, we describe a setup that allows the calibration of the transresistance gain of these ultralow-current transresistance amplifiers. The setup is intended to fill a traceability and accuracy gap between the manufacturer gain specifications (gain tolerance relative to the nominal value in the 10^{-2} range), and the uncertainty level that can achieved with primary metrology experiments based on CCCs.

The setup is based on the capacitance-charging method, which allows to generate accurate currents (typically ranging from $100\,\mathrm{fA}$ to $1\,\mathrm{nA}$) by applying a linear voltage ramp on a differentiating capacitor.[1] The method is insensitive to nonidealities of the input stage of the instrument being calibrated, such as the voltage burden and a finite input resistance. Several implementations of the method, focused on the calibration of the reading error of low-current meters with display output [12]–[19] were proposed and mutually verified in an international intercomparison [20].

The setup here proposed performs a calibration of the gain R of a transresistance amplifier, traceable to the capacitance of a gas-dielectric capacitor C and to the period T of a low-frequency timebase. No absolute voltage traceability of the instruments employed is needed. Two different calibration modes have been tested: a *dc current mode*,[2] and a *sinewave current mode*, using a very low-frequency sine current signal. The dc current mode requires a custom-made voltage source, and is more accurate; the sinewave current mode can be more easily implemented, using only commercially available equipment. In both cases, the resulting setup configuration is low-cost, simple, compact, and easy to use; it is possible to embed the entire calibration setup within the main electron counting experiments, and thus achieve quasi-in-line calibrations of R.

We provide an example of calibration of a specific amplifier model (FEMTO mod. DDPCA-300), which is popular in electron counting [8]–[10], [22] and nanophysics experiments [23], [24]. For this amplifier model the setup allows to calibrate, in the direct current mode, the transresistance gain at the nominal setting of $10\,\mathrm{G\Omega}$ with a relative uncertainty of a few parts in 10^5.

II. Principle of operation

The operating principle of the calibration setup is shown in Fig. 1. The voltage $v_{\mathrm{in}}(t)$ is applied to a differentiating capacitor to generate the test current

$$i(t) = C\frac{\mathrm{d}v_{\mathrm{in}}(t)}{\mathrm{d}t} \tag{1}$$

I. Finardi and L. Callegaro are with the Istituto Nazionale di Ricerca Metrologica (INRiM), 10135 Torino, Italy. (e-mail: i.finardi@inrim.it)
I. Finardi is with Politecnico di Torino, 10129 Torino, Italy.

[1]The earliest reference to this method for metrological purposes the authors are aware of is [11].

[2]Preliminary tests using this excitation were presented in [21].

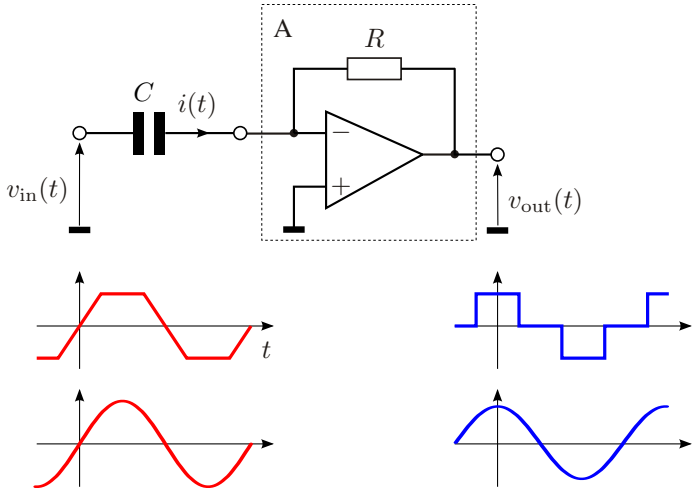

Fig. 1. Principle schematic diagram of the calibration setup, as described in Sec. II. The current $i(t)$ is generated from voltage $v_{\mathrm{in}}(t)$ by the injection capacitor C; the amplifier A, with transresistance R (here ideally associated to its feedback resistance) generates the output voltage $v_{\mathrm{out}}(t)$. The waveform pictured for $v_{\mathrm{in}}(t)$ (—) and $v_{\mathrm{out}}(t)$ (—) are associated to the two different calibration modes proposed in the paper.

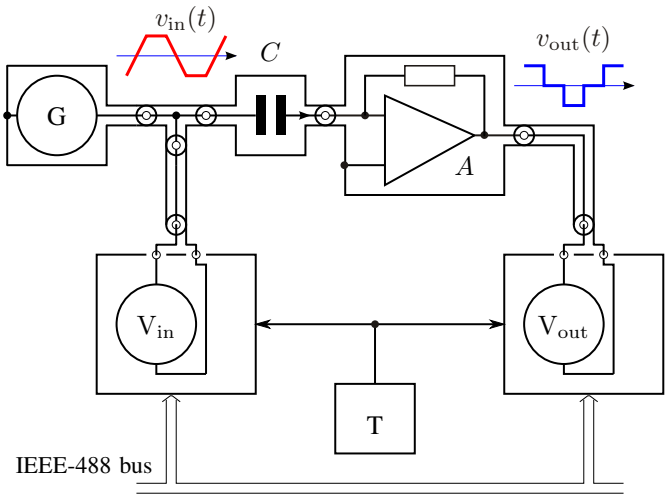

Fig. 2. Schematic diagram of the calibration setup, see Sec. III-A for a description. The waveform shapes $v_{\mathrm{in}}(t)$ and $v_{\mathrm{out}}(t)$ displayed correspond to the dc current calibration mode.

The amplifier A, whose transresistance gain R has to be calibrated, generates an output voltage $v_{\mathrm{out}}(t) = Ri(t)$, hence the relation

$$R^{-1} = C\frac{1}{v_{\mathrm{out}}(t)}\frac{\mathrm{d}v_{\mathrm{in}}(t)}{\mathrm{d}t} \tag{2}$$

holds.

Eq. (2) shows that the traceability of the measurement of R is given by C, a timebase, and a voltage *ratio*; therefore, absolute voltage traceability is not required.[3]

III. Implementation

A. Setup

The schematic diagram of the calibration setup is shown in Fig. 2, and a photograph of the same is given in Fig. 3. The source G generates the voltage $v_{\mathrm{in}}(t)$, which is applied to the capacitor C. The capacitor generates the displacement current $i(t)$, in agreement with (1). $i(t)$ is injected to the input of the transresistance amplifier A to be calibrated. Both the input voltage $v_{\mathrm{in}}(t)$ and the output voltage $v_{\mathrm{out}}(t)$ are sampled at regular intervals by the voltmeters $\mathrm{V_{in}}$ and $\mathrm{V_{out}}$, synchronized by

[3]The method here proposed is a derivation of a method developed for the calibration of low-current meters [14], [19], where a proper traceability of the $v_{\mathrm{in}}(t)$ measurement was however necessary.

Fig. 3. A photo of the calibration setup corresponding to the schematic diagram of Fig. 2. The source G (for the dc current calibration mode) is on the bottom left; C and A in the center; $\mathrm{V_{in}}$ on top left; $\mathrm{V_{out}}$ on the right. A detail of C and A is given in Fig. 4.

the same trigger signal T. The samples of $v_{\mathrm{in}}(t)$ and $v_{\mathrm{out}}(t)$ are acquired by a computer through an interface bus (IEEE-488) for off-line processing.

As shown in Fig. 3, the whole circuit is wired by coaxial cables. To reduce possible effects of cable dielectric absorption, C and A are connected directly, without any cable, as can be seen in Fig. 4.

B. Calibration modes

Two calbration modes have been investigated, differing in the waveform of the current $i(t)$ being generated, and, consequently, of $v_{\mathrm{in}}(t)$: a *direct current mode*, which requires a purpose-built voltage generator, and a *sinewave current mode* at a very low angular frequency ω, which can be achieved with a suitable commercial generator, and is therefore easier to implement.

Direct current: (1) shows that a linear voltage ramp $v_{\mathrm{in}}(t) = Kt$, where K is the voltage slope, generates a constant current I. In such a steady-state regime, the constant voltage burden on A (caused by the non-zero input impedance, and by offsets) does not alter the ramp slope, and hence has no effect on the value of I.
To achieve this calibration mode, the waveform shape of $v_{\mathrm{in}}(t)$ generated by G has a symmetric trapezoidal shape with a very long period, as can be seen in Fig. 5. Such piecewise linear waveform includes three different voltage slopes (positive, negative and zero) which correspond to three different nominal calibration current values $+I_{\mathrm{nom}}$, $-I_{\mathrm{nom}}$ and $I = \pm 0$. The current value $I = 0$ allows to determine the offset of A in the course of the measurement.

Sinewave current: if ω and the amplifier time constant τ satisfy the relation $\omega\tau \ll 1$, the measured complex transimpedance $Z(\omega) = R(\omega) + \mathrm{j}X(\omega)$ can be written as

$$Z(\omega) \approx R(0)\left(1 - (\omega\tau)^2 - \mathrm{j}\omega\tau\right) \tag{3}$$

and therefore the quantity of interest, the dc transresistance gain $R(0)$, can be approximated by the measured $R(\omega)$ to the second order in $\omega\tau$.

Fig. 4. Detail of setup, showing the direct connection (no cable) of the injection capacitor C (on the left) to the transresistance amplifier A (center of the picture) to minimize currents related to the dielectric absorption in the connection insulators.

TABLE I
INJECTION CAPACITOR MODELS EMPLOYED IN THE CALIBRATION SETUP, LISTED BY NOMINAL CAPACITANCE C_{nom}.

C_{nom}	Model
1 pF	General Radio mod. 1403-K
10 pF	Sullivan mod. C80001
100 pF	Sullivan mod. C80002
1 nF	General Radio mod. 1404-A [33]

C. Instrumentation

1) Voltage generator: Two different signal generators have been employed for the two calibration modes described in Sec. III-B.

Direct current: G is a purpose-built voltage source. The generated signal $v_{\mathrm{in}}(t)$ has a maximum span of $\pm 10\,\mathrm{V}$, and the ramp sections of the trapezoidal waveform have slopes of about $\pm 0.1\,\mathrm{V\,s^{-1}}$ (adjustable). The positive and negative voltage ramp phases have a duration of $\approx 200\,\mathrm{s}$ each; the phases of constant voltage also have a duration of $\approx 200\,\mathrm{s}$. Hence, the total period of one $v_{\mathrm{in}}(t)$ cycle is $\approx 800\,\mathrm{s}$. The source is based on analog electronics; it is battery-powered and free-running (thus requiring no control signal), in order to achieve complete galvanic isolation and help to reduce the interferences in the calibration circuit. The source output is generated by an analog pure integrator, which is driven by a three-state (positive, zero, negative) constant current source of adjustable amplitude. The loss in the integrating dielectric capacitor are compensated with an active feedback network, which is manually adjusted in order to achieve the maximum linearity of the voltage ramps. A more complete description of the source is given in Ref. [14].

Sinewave current: G is a Stanford mod. DS360 low-distortion ($< 100\,\mathrm{dB}$) function generator, typically operated at $f \approx 3\,\mathrm{mHz}$ (measured with a frequency meter).

2) Injection capacitor: C has to be a gas-dielectric (or vacuum) capacitance standard, because all solid-dielectric capacitors show the phenomenon of dielectric absorption [25], which give deviations from (1).

For the current range investigated, commercial standard capacitors having nominal values $C_{\rm nom}$ from $1\,\mathrm{pF}$ to $1000\,\mathrm{pF}$ are adequate. The specific models employed are listed in Table I. The capacitors were modified to employ low-dielectric-absorption connectors (Teflon insulation); for the same reason, the solid-dielectric trimming capacitors were removed.

The value of C is measured as a two terminal-pair standard [26, Ch. 2] with a commercial capacitance bridge (Andeen-Hagerling mod. 2500A) at the frequency of $1\,\mathrm{kHz}$. The calibration is traceable to the Italian national standard of electrical capacitance.

Residual frequency dependence in gas-dielectric capacitors has been observed, and ascribed to surface effects [27]–[29]. It has been shown [28] that the capacitance value at very low frequency can be predicted by extrapolation from measurements in the in the audio frequency range ($20\,\mathrm{Hz} - 1\,\mathrm{kHz}$). For the specific items employed, the prediction suggests a relative deviation lower than $10{\times}10^{-6}$.

3) Voltmeters: $\mathrm{V_{in}}$ is an Agilent mod. 3458A multimeter, whose acquisition is in dc sampling mode, with the autozero and autorange functions disabled. $\mathrm{V_{out}}$ is an Agilent mod. 34401A multimeter, also configured for dc sampling. Both these voltmeters are in external trigger mode, and are synchronously triggered by a precision timer T, at the sampling frequency of $\approx 950\,\mathrm{mHz}$. All samples are acquired via the IEEE-488 bus and off-line processed. Although not required by the proposed method (see discussion in Sec. II), the voltmeters are routinely calibrated, with traceability to the Italian national standard of dc voltage.

D. Data processing

Sampled values of $v_{\rm in}(t)$ and $v_{\rm out}(t)$ are processed in different ways depending on the calibration mode chosen.

Direct current: after identification of the samples belonging to the different waveform slopes, a finite-difference version of (1) is computed from the samples of $v_{\rm in}(t)$, $v_{\rm out}(t)$. Details are given in [14]. For typical measurement settings, the V resolution (8 digits) and the use of double-precision floating-point arithmetics make quantization and numerical rounding errors negligible.

Sinewave current: the waveforms $v_{\rm in}(t)$ and $v_{\rm out}(t)$ are modeled as

$$\begin{aligned} v_{\rm in}(t) &= A_{\rm in}\cos(\omega t) + B_{\rm in}\sin(\omega t) + C_{\rm in}, \\ v_{\rm out}(t) &= A_{\rm out}\cos(\omega t) + B_{\rm out}\sin(\omega t) + C_{\rm out}, \end{aligned} \tag{4}$$

whose parameters are identified by processing the sampled values with a seven-parameter sine-fitting algorithm [30]. The voltage transfer function Q is computed as

$$Q = \frac{1}{Q_{\rm c}}\frac{V_{\rm out}}{V_{\rm in}} = \frac{1}{Q_{\rm c}}\frac{A_{\rm out} + \mathrm{j}B_{\rm out}}{A_{\rm in} + \mathrm{j}B_{\rm in}}, \tag{5}$$

where $Q_{\rm c}$ is a calibration factor to compensate for the different ac response of the two voltmeters $\mathrm{V_{in}}$ and $\mathrm{V_{out}}$: it can be determined by measuring the same signal $v_{\rm in}(t)$ with both voltmeters in parallel.

The complex transresistance gain $Z(\omega)$ is then computed as $Z(\omega) = \dfrac{Q}{\mathrm{j}\,\omega C}$. The approximation of Eq. (3) can then be taken in consideration.

E. Device under test

The calibration setup was tested with a FEMTO mod. DDPCA-300 transresistance amplifier as A. The amplifier has a nominal transresistance gain $R_{\rm nom}$ manually switchable from $10\,\mathrm{k\Omega}$ to $10\,\mathrm{T\Omega}$ and is specified to be stable for capacitances at the input up to $10\,\mathrm{nF}$, therefore for all capacitance standards of Tab. I. The output voltage range is $\pm 10\,\mathrm{V}$; the current noise is dependent on $R_{\rm nom}$ and reaches $200\,\mathrm{aA\,Hz^{-\frac{1}{2}}}$ in the highest gain ranges. The specified accuracy of $R_{\rm nom}$ is $\pm 1\,\%$. The specified gain temperature coefficient is $1{\times}10^{-4}\,\mathrm{K^{-1}}$ to $3{\times}10^{-4}\,\mathrm{K^{-1}}$ depending on the range, although the latter value seems overestimated (see Sec. IV-C). The amplifier surface temperature is monitored and, after an initial settling, it is stable to better than $0.1\,\mathrm{K}$ for the whole measurement period. The amplifier has a configurable output lowpass filter; all measurements reported were performed in the so-called *full bandwidth* mode, which is $1\,\mathrm{Hz}$ to $20\,\mathrm{Hz}$ in the gain range investigated.

IV. Results

To avoid possible systematic error in the calibration caused by noise clipping, the calibration currents ($\pm I_{\rm nom}$ for the dc calibration mode, the peak value for the sinewave calibration mode) are chosen to be slightly lower (in absolute value) than the corresponding decadic value. In particular, the $I_{\rm nom}$ values chosen are: $\pm 0.95\,\mathrm{pA}$, $\pm 9.5\,\mathrm{pA}$, and $\pm 95\,\mathrm{pA}$.

All measurements were performed in a shielded and thermostated $(23.0(5)\,^{\circ}\mathrm{C})$ room.

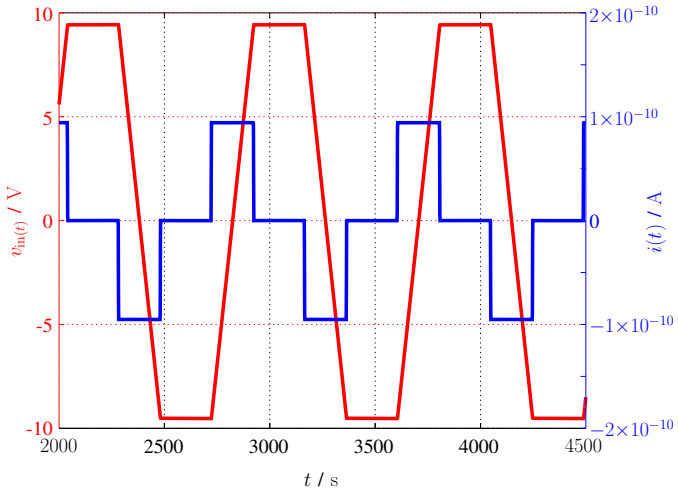

Fig. 5. The outcome of a typical measurement ($R_{\mathrm{nom}} = 10\,\mathrm{G\Omega}$, $C_{\mathrm{nom}} = 1\,\mathrm{nF}$, $I_{\mathrm{nom}} = 95\,\mathrm{pA}$). Red line (—) is the trapezoidal ramp signal $v_{\mathrm{in}}(t)$; blue line (—) is the test current $i(t)$. The sign of $i(t)$ is determined by the sign of the slope of $v_{\mathrm{in}}(t)$; when $v_{\mathrm{in}}(t)$ is constant, $i(t) = 0$.

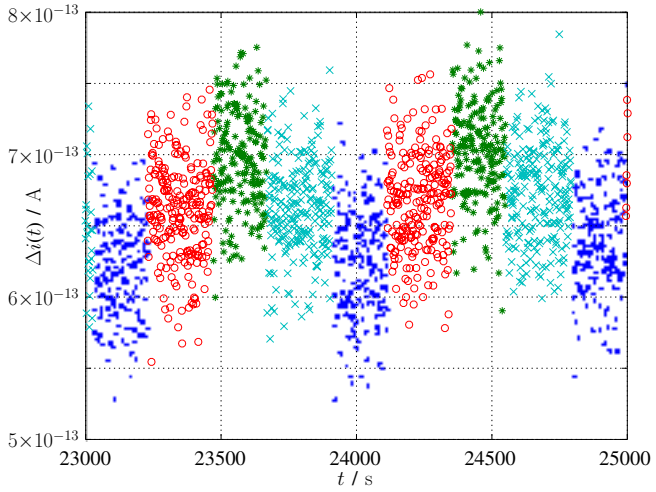

Fig. 6. Time sequence of the amplifier equivalent error the input $\Delta i(t)$ (see Sec. IV for the definition). The four different symbols correspond to the four different phases of $v_{\mathrm{in}}(t)$. • corresponds to $v_{\mathrm{in}}(t)$ positive ramp slope, and to $i(t) = +I_{\mathrm{nom}}$. ∗ negative ramp slope, $i(t) = -I_{\mathrm{nom}}$. ○ $v_{\mathrm{in}}(t)$ constant positive, $i(t) = +0$. × $v_{\mathrm{in}}(t)$ constant negative, $i(t) = -0$. The offset of A is computed from the average of the $i(t) = +0$ and $i(t) = -0$ phases.

A. Direct current mode

The setup has been employed to calibrate the transresistance nominal settings $R_{\mathrm{nom}} = 10\,\mathrm{G\Omega}$, $100\,\mathrm{G\Omega}$, $1\,\mathrm{T\Omega}$ and $10\,\mathrm{T\Omega}$ of A. Each calibration was performed by running the system for about 50 cycles of $v_{\mathrm{in}}(t)$, corresponding to a total measurement time of 10 h. The calibration strategy and the related acquisition, data processing software and uncertainty analysis is described in [14], [20].

The measurement example of Fig. 5, 6 and 7 refers to the following calibration conditions: $R_{\mathrm{nom}} = 10\,\mathrm{G\Omega}$, $C_{\mathrm{nom}} = 1\,\mathrm{nF}$, $I_{\mathrm{nom}} = \pm 95\,\mathrm{pA}$.

Fig. 5 shows the time series of the samples of $v_{\mathrm{in}}(t)$ (measured by $\mathrm{V_{in}}$) and of $i(t)$ as determined by (1) over a few measurement cycles.

Fig. 6 displays the amplifier equivalent error at the input $\Delta i(t) = R_{\mathrm{nom}}^{-1} v_{\mathrm{out}}(t) - i(t)$, here defined as the deviation of the current reading $R_{\mathrm{nom}}^{-1} v_{\mathrm{out}}(t)$ (computed from the amplifier voltage output $v_{\mathrm{out}}(t)$ with the nominal transresistance R_{nom}), and the calibration current $i(t)$.

Fig. 7 shows the transresistance gain relative deviation from nominal $\delta R = (R - R_{\mathrm{nom}})/R_{\mathrm{nom}}$ evaluated for each positive and negative semicycles of $v_{\mathrm{in}}(t)$. The mean and the standard deviation of R for each time series corresponding to Fig. 7 give the calibration outcome for each nominal current sign. The outcome of the calibration for different test currents and nominal transresistance of the amplifier is reported in Tab. II. For the nominal transresistance values $R_{\mathrm{nom}} = 1\,\mathrm{T\Omega}$ and $10\,\mathrm{T\Omega}$ the calibration is performed with two different test currents. For $R_{\mathrm{nom}} = 1\,\mathrm{T\Omega}$ significant differences occur between the δR values

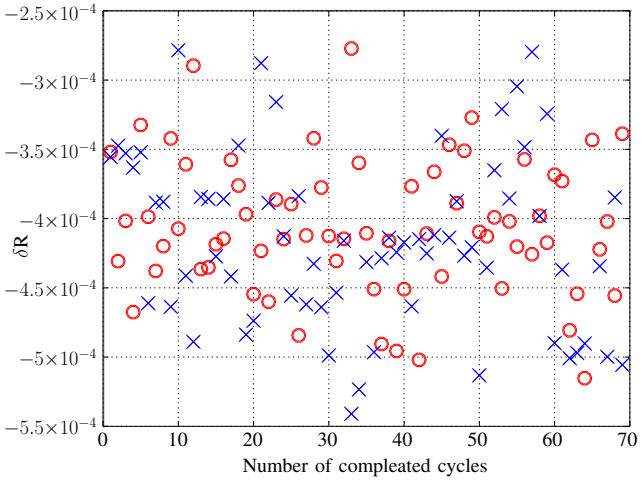

Fig. 7. The amplifier transresistance gain error $\delta R = (R - R_{\rm nom})/R_{\rm nom}$ versus measurement time, evaluated for each positive (○) and negative (×) semicycle of $v_{\rm in}(t)$.

TABLE II
RESULTS OF THE TRANSRESISTANCE AMPLIFIER CALIBRATION USING DIRECT CURRENT

$R_{\rm nom}$	$I_{\rm nom}$	$C_{\rm nom}$	δR
10 GΩ	95 pA −95 pA	1 nF	$-4.35(35)\times10^{-4}$ $-4.62(40)\times10^{-4}$
10 GΩ	9.5 pA −9.5 pA	100 pF	$-4.64(34)\times10^{-4}$ $-4.54(59)\times10^{-4}$
100 GΩ	9.5 pA −9.5 pA	100 pF	$-3.05(3)\times10^{-3}$ $-3.09(4)\times10^{-3}$
1 TΩ	9.5 pA −9.5 pA	100 pF	$-2.90(3)\times10^{-3}$ $-4.32(3)\times10^{-3}$
1 TΩ	0.95 pA −0.95 pA	10 pF	$-3.29(9)\times10^{-3}$ $-3.14(7)\times10^{-3}$
10 TΩ	0.95 pA −0.95 pA	10 pF	$-5.77(8)\times10^{-3}$ $-5.76(6)\times10^{-3}$
10 TΩ	0.095 pA −0.095 pA	1 pF	$-5.83(18)\times10^{-3}$ $-6.03(2)\times10^{-3}$

obtained with different current magnitudes and sign; these discrepancies deserve further investigation.

An example of uncertainty budget for the calibration point $R_{\rm nom} = 10\,{\rm G\Omega}$, $I_{\rm nom} = \pm 95\,{\rm pA}$ is reported in Table III. The uncertainty contributions related to the readings of $V_{\rm in}$ and $V_{\rm out}$ are not reported, since these can be reduced (below parts in 10^6) by a mutual calibration of the two voltmeters, see Sec. II. The budget is dominated by contributions related to C: these can be reduced by embedding the capacitor in a thermostat, and with a better calibration, including a more thorough investigation of its frequency dependence (see Sec. III-C2).

TABLE III
UNCERTAINTY BUDGET FOR $R_{\rm nom} = 10\,{\rm G\Omega}$, $C_{\rm nom} = 1\,{\rm nF}$, $I_{\rm nom} = \pm 95\,{\rm pA}$.

	Source	Contribution to $u(\delta{\rm R})$	Type
	C calibration, frequency and temperature dependence	3.0×10^{-5}	B
	V_{in} sampling	5.0×10^{-6}	B
	Timebase T accuracy	1.0×10^{-6}	B
	C current leakages	1.0×10^{-5}	B
$I_{\rm nom} = +95\,{\rm pA}$	Reading noise	9.5×10^{-6}	A
$I_{\rm nom} = -95\,{\rm pA}$	Reading noise	1.6×10^{-5}	A
$I_{\rm nom} = +95\,{\rm pA}$	$u(\delta{\rm R}) =$	3.4×10^{-5}	RSS
$I_{\rm nom} = -95\,{\rm pA}$	$u(\delta{\rm R}) =$	3.6×10^{-5}	RSS

TABLE IV
COMPARISION BETWEEN THE TWO DIFFERENT CALIBRATION WAVEFORMS

R_{nom}	I_{nom}	C_{nom}	δR	
			direct current	sinewave
$10\,\mathrm{G\Omega}$	$95\,\mathrm{pA}$	$1\,\mathrm{nF}$	$-4.49(27)\times10^{-4}$	$-3.89(40)\times10^{-4}$
$10\,\mathrm{G\Omega}$	$9.5\,\mathrm{pA}$	$100\,\mathrm{pF}$	$-4.59(34)\times10^{-4}$	$-3.84(38)\times10^{-4}$
$100\,\mathrm{G\Omega}$	$9.5\,\mathrm{pA}$	$100\,\mathrm{pF}$	$-3.07(3)\times10^{-3}$	$-3.00(5)\times10^{-3}$

B. Sinewave current mode

The calibration has been performed on the nominal gain values R_{nom} =10 GΩ and 100 GΩ, with sinusoidal currents of frequency $f \approx 3\,\mathrm{mHz}$ and peak values I_{nom} =9.5 pA and 95 pA.

Fig. 8 shows an excerpt of the time series of sampled $v_{\mathrm{in}}(t)$ and $v_{\mathrm{out}}(t)$ waveforms in the case of R_{nom} =10 GΩ and C_{nom} =1 nF . The figure shows also the residuals after fitting with model (4).

The outcome of the calibration is reported in Table IV. The uncertainty sources are similar to the dc current method reported in Table III, to which a contribution related to the fitting residuals shown in Fig. 8 has to be added. A proper expression of such uncertainty contribution goes beyond the scope of this paper, an overestimation of 2×10^{-5} has been included in the budget.

C. In-use uncertainty

The calibrated transresistance gain value R obtained with the setup can be directly employed in current measurement experiments. As customary the calibration uncertainties reported in Tab. II, III, IV do not consider the in-use uncertainty contributions, which are dependent on the specific experiment where the amplifier is employed, and can include:

- Gain environmental drifts. For the amplifier model considered, in the range probed with the setup, the gain temperature coefficient is specified by the manufacturer as $3\times10^{-4}\,\mathrm{K}^{-1}$, although, for the specific item investigated, our preliminary measurements give an upper limit of $1\times10^{-5}\,\mathrm{K}^{-1}$ at $R_{\mathrm{nom}} = 10\,\mathrm{T\Omega}$. This in-use uncertainty contributions will be strongly mitigated by quasi-in-line implementations.
- Amplifier nonlinearity. The direct-current mode allows a calibration on the specific current value to be measured, or (with much more experimental effort) the determination of a calibration curve, for which a general estimation method [31] of the measurand and its uncertainty can be applied. The ac-current calibration mode gives an average gain value over the span of the input current, and is not suited for such an advanced data treatment. For the particular amplifier item investigated, the nonlinearity magnitude can be inferred from results given in Tab. II.
- Noise, including the noise of the current being measured (flicker and shot noise), and the quantization noise of A voltage output reading, if performed with a low-resolution instrument.

An estimate of in-use uncertainty components requires detailed information about the specific measurement environment where the calibrated amplifier is embedded.

For higher gain and lower currents, noise is the dominant contribution to uncertainty. To give an example, a measurement current of $100\,\mathrm{fA}$ generated by a $1\,\mathrm{G\Omega}$ resistor at $100\,\mathrm{mK}$ has an intrinsic noise (Johnson + shot) of $0.2\,\mathrm{fA\,Hz^{-1/2}}$. The ULCA-1 [6, Sec. IV] has an equivalent input noise current at $1\,\mathrm{Hz}$ of $2.4\,\mathrm{fA\,Hz^{-1/2}}$, while the FEMTO DDPCA-300 here tested is specified at $0.2\,\mathrm{fA\,Hz^{-1/2}}$. Environmental interferences, for example caused by a dry cryostat, can easily increase the measurement noise of one order of magnitude [10, Fig. 4].

V. DISCUSSION AND CONCLUSIONS

The proposed setup can calibrate the transresistance gain of amplifiers suitable for the measurement of ultralow-valued dc currents. The method is simple and can be embedded in an electron-counting experiment with relative ease. As Eq. (2) shows, the method requires traceability to capacitance and time units, since it involves only voltage ratios.

The two calibration modes presented provide different measurand definitions and therefore cannot be directly compared. Even under the assumption (3), the direct current mode probes A on single dc values, whereas the sinewave current mode gives an average of δR over the whole sinewave span. Nevertheless, the values given in Table IV show that the measurement outcomes are comparable within the combined uncertainties.

The uncertainty achieved in the calibration process is one or two order of magnitudes better than typical manufacturer specifications for these amplifier, and comparable — for same nominal currents — with that achieved by published setups for calibration of low-current meters with a display output [12], [13], [15], [32]; these setups, however, ask for absolute voltage traceability. Lower calibration uncertainties than those here presented can be achieved, but with more demanding experiments which include current ratio measurements with CCCs [4]–[7].

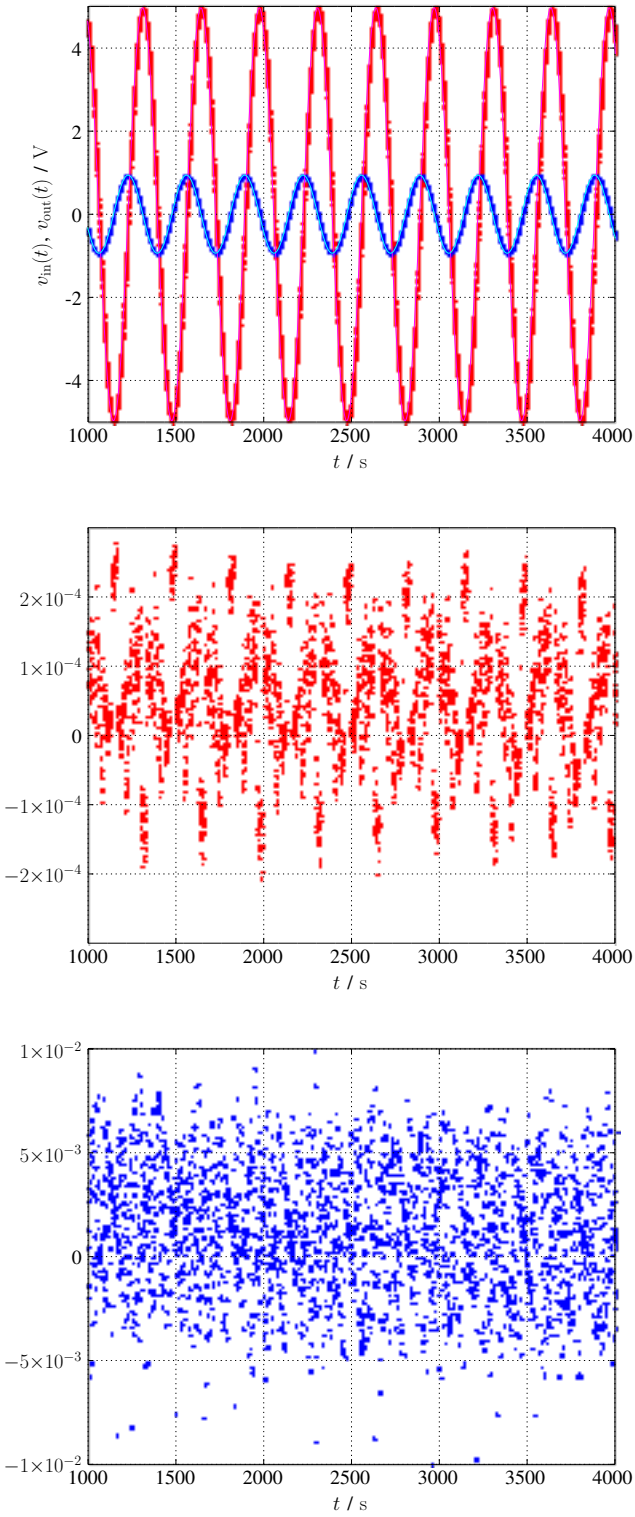

Fig. 8. Example of the outcome of a measurement, for the case $R_{\rm nom}$ = 10 GΩ and $C_{\rm nom}$ = 1 nF. (top) Time series of sampled signals $v_{\rm in}(t)$ (—) and $v_{\rm out}(t)$ (—). (middle, •) Residuals of the seven-parameter fitting on $v_{\rm in}(t)$, showing the distortion of G. (bottom, •) Fit residuals of $v_{\rm out}(t)$, dominated by the noise of A.

VI. Acknowledgments

The authors are indebted with Vincenzo D'Elia, INRIM, for help in the realization of the measurement setup; Massimo Ortolano, Politecnico di Torino, for fruitful dicussions; and with Luca Croin, INRIM, for the photographic material.

References

[1] Bureau International des Poids et Mesures, "The International System of Units," Dec 2015, draft of the 9th SI Brochure. [Online]. Available: www.bipm.org

[2] CCEM WGSI, "Mise en pratique for the ampere and other electric units in the International System of units (SI)," 2017, draft 4. [Online]. Available: www.bipm.org

[3] F. Gay, F. Piquemal, and G. Geneves, "Ultralow noise current amplifier based on a cryogenic current comparator," *Rev. Sci. Instrum.*, vol. 71, no. 12, pp. 4592–4595, 2000.

[4] G. Rietveld, E. Bartolomé, J. Sesé, P. de la Court, J. Flokstra, C. Rillo, and A. Camón, "1:30 000 cryogenic current comparator with optimum squid readout," *IEEE Trans. Instr. Meas.*, vol. 52, no. 2, pp. 621–625, 2003.

[5] D. Drung, M. Götz, E. Pesel, and H. Scherer, "Improving the traceable measurement and generation of small direct currents," *IEEE Trans. Instrum. Meas.*, vol. 64, no. 11, pp. 3021–3030, 2015.

[6] D. Drung, C. Krause, U. Becker, H. Scherer, and F. Ahlers, "Ultrastable low-noise current amplifier: A novel device for measuring small electric currents with high accuracy," *Rev. of Sci. Instrum.*, vol. 86, no. 2, p. 024703, 2015.

[7] D. Drung, C. Krause, S. P. Giblin, S. Djordjevic, F. Piquemal, O. Séron, F. Rengnez, M. Götz, E. Pesel, and H. Scherer, "Validation of the ultrastable low-noise current amplifier as travelling standard for small direct currents," *Metrologia*, vol. 52, no. 6, p. 756, 2015.

[8] J. Lehtinen, "Quantum fluctuations in superconducting nanostructures," Ph.D. dissertation, iSBN: 978-951-39-5688-9. [Online]. Available: http://www.jyu.fi/static/fysiikka/vaitoskirjat/2014/Lehtinen-Janne-2014.pdf

[9] A. Rossi, T. Tanttu, K. Y. Tan, I. Iisakka, R. Zhao, K. W. Chan, G. C. Tettamanzi, S. Rogge, A. S. Dzurak, and M. Möttönen, "An accurate single-electron pump based on a highly tunable silicon quantum dot," *Nano lett.*, vol. 14, no. 6, pp. 3405–3411, 2014.

[10] E. Mykkänen, J. Lehtinen, A. Kemppinen, C. Krause, D. Drung, J. Nissilä, and A. Manninen, "Reducing current noise in cryogenic experiments by vacuum-insulated cables," *Rev. Sci. Instrum.*, vol. 87, no. 10, p. 105111, 2016.

[11] T. B. Rozhdestvenskaya, D. I. Antonova, O. M. Pavlov, L. M. Stepanova, O. V. Saks, V. S. Grafov, V. A. Matrosov, and A. V. Pokrovskaya, "New methods and standard equipment fo the metrological assurance of insrumentation for measurements of extremely low d.c. currents," in *Proceedings of the 8th IMEKO Congress of the International Measurement Confederation*, ser. Measurement for progress in science and technology, G. Striker, J. Solt, and T. Kemeny, Eds., vol. Acta IMEKO 1979, IMEKO. North-Holland USSR, 21-27 May 1980, pp. 751–756.

[12] G.-D. Willenberg, H. N. Tauscher, and P. Warnecke, "A traceable precision current source for currents between 100 aA and 10 pA," *IEEE Trans. Instr. Meas.*, vol. 52, no. 2, pp. 436–439, Apr. 2003.

[13] H. van den Brom, P. de la Court, and G. Rietveld, "Accurate subpicoampere current source based on a differentiating capacitor with software-controlled nonlinearity compensation," *IEEE Trans. Instr. Meas.*, vol. 54, no. 2, pp. 554–558, Apr. 2005.

[14] L. Callegaro, V. D'Elia, and B. Trinchera, "A current source for picoammeter calibration," *IEEE Trans. Instr. Meas.*, vol. 56, no. 4, pp. 1198–1201, Aug. 2007.

[15] N. E. Fletcher, S. P. Giblin, J. M. Williams, and K. J. Lines, "New capability for generating and measuring small DC currents at NPL," *IEEE Trans. Instr. Meas.*, vol. 56, no. 2, pp. 326–330, Apr. 2007.

[16] I. Iisakka, K. Kalliomäki, J. Seppälä, and A. Manninen, "Subpicoampere current source based on a digital-to-analog converter," in *Conference on Precision Electromagnetic Measurements (CPEM) Digest*, Broomfield, CO, USA, Jun 8-13 2008, pp. 352–353.

[17] G.-D. Willenberg and H. N. Tauscher, "Novel digital voltage ramp generator for use in precision current sources in the picoampere range," *IEEE Trans. Instr. Meas.*, vol. 58, no. 4, pp. 756–760, Apr. 2009.

[18] T. Bergsten, K.-E. Rydler, O. Gunnarsson, G. Eklund, and V. Tarasso, "A precision current source using $\Delta - \Sigma$ modulation," *IEEE Trans. Instr. Meas.*, vol. 60, no. 7, pp. 2341–2346, July 2011.

[19] L. Callegaro, P. P. Capra, V. D'Elia, and F. Galliana, "Generation of reference DC currents at 1 nA level with the capacitance charging method," *IEEE Trans. Instr. Meas.*, vol. 63, no. 7, pp. 1779–1782, Jul. 2014.

[20] G.-D. Willenberg, "EUROMET.EM-S24: Supplementary comparison of small current sources," *Metrologia*, vol. 50, no. 1A, p. 01002, 2013.

[21] I. Finardi and L. Callegaro, "Calibration setup for ultralow-current transresistance amplifiers," vol. 2017 IEEE International Instrumentation and Measurement Technology Conference, Torino, Italy, May 22, 25 2017, in press. See also arXiv:1610.05148.

[22] S. Nakamura, Y. A. Pashkin, J.-S. Tsai, and N.-H. Kaneko, "Single-electron pumping by parallel SINIS turnstiles for quantum current standard," *IEEE Transactions on Instrumentation and Measurement*, vol. 64, no. 6, pp. 1696–1701, 2015.

[23] R. S. Popovic and M. Lany, "Electrical measurements in nanotechnology using single electron bipolar avalanche transistors," in *Proc. MIEL*. IEEE, 2010, pp. 51–56.

[24] G. Cheng, J. P. Veazey, P. Irvin, C. Cen, D. F. Bogorin, F. Bi, M. Huang, S. Lu, C.-W. Bark, S. Ryu *et al.*, "Anomalous transport in sketched nanostructures $LaAlO_3/SrTiO_3$ at the interface," *Phys. Rev. X*, vol. 3, no. 1, p. 011021, 2013.

[25] R. A. Pease, "Understand capacitor soakage to optimize analog systems," *Electronic Design*, pp. 125–129, 1982.

[26] L. Callegaro, *Electrical impedance: principles, measurement, and applications*, ser. in Sensors. Boca Raton, FL, USA: CRC press: Taylor & Francis, 2013, iSBN: 978-1-43-984910-1.

[27] B. D. Inglis, "Frequency dependence of electrode surface effects in parallel-plate capacitors," *IEEE Trans. Instr. Meas.*, vol. 24, pp. 133–150, Jun 1975.

[28] S. P. Giblin, G. D. Willenberg, and N. E. Fletcher, "Frequency dependence of gas-dielectric capacitors used in sub-nA reference current generators," in *Conference on Precision Electromagnetic Measurements (CPEM) Digest*, Daejeon, Korea, Jun 13-18 2010, pp. 318–319.

[29] G. Rietveld, N. Zimmerman, and H. van den Brom, "First experimental results of the frequency dependence of a vacuum-gap capacitor between 1 kHz and 0.02 Hz," in *Conference on Precision Electromagnetic Measurements (CPEM) Digest*, Jul. 2012, pp. 708 –709.

[30] P. M. Ramos and A. C. Serra, "A new sine-fitting algorithm for accurate amplitude and phase measurements in two channel acquisition systems," *Measurement*, vol. 41, no. 2, pp. 135–143, 2008.

[31] W. Bich and F. Pennecchi, "On the in-use uncertainty of an instrument," in *Advanced Mathematical and Computational Tools in metrology*, P. Ciarlini, M. G. Fox, F. Pavese, and G. B. Rossi, Eds. Singapore: Woirld Scientific, 2004, vol. VI, pp. 159–169.

[32] L. Callegaro, V. D'Elia, P. P. Capra, and A. Sosso, "Techniques for traceable measurements of small currents," *IEEE Trans. Instr. Meas.*, vol. 56, no. 2, pp. 295–299, Apr. 2007.

[33] J. Hersh, "A highly stable reference standard capacitor," *General Radio Experim.*, vol. 37, no. 8, pp. 1–8, 1963.

Ilaria Finardi (1990) obtained her Master's Degree in Physics in 2015 from Università di Torino, Italy. Since then she is a Ph. D. student at Politecnico di Torino in collaboration with the Istituto Nazionale di Ricerca Metrologica, INRIM, Torino, Italy. Her research interests are focused on single electron devices: fabrication and measurements.

Luca Callegaro (1967) holds a degree in Electronic Engineering (1992) and a Ph. D. in Physics (1996), both from Politecnico di Milano, Italy. He joined the Istituto Nazionale di Ricerca Metrologica, INRIM (formerly Istituto Elettrotecnico Nazionale Galileo Ferraris, IEN), Torino, Italy, in 1996. He has been member of the Scientific Council of IEN (1998-2005), and adjunct professor of electronic measurements at Politecnico di Torino. He is presently head of the Nanoscience and Materials Division of INRIM: his research interests are focused on electrical impedance, and he is responsible of the Italian National standards of electrical capacitance, inductance, ac resistance and ac voltage ratio. He is chairman of the Technical Committee for Electricity and Magnetism (TC-EM) of EURAMET, the European Association of National Metrology Institutes. He is author of about 80 papers on international reviews and of the book *Electrical impedance: principles, measurement and applications*, CRC Press: Taylor and Francis.